Dynamic Properties of Lightweight Cellular Concrete for Geotechnical Applications

Binod Tiwari, M.ASCE[1]; Beena Ajmera, A.M.ASCE[2]; and Diego Villegas[3]

Abstract: Lightweight cellular concrete (LCC) materials have been used in various civil engineering applications for several decades. In this study, the dynamic behavior of LCC materials was evaluated for possible geotechnical applications, such as mechanically stabilized earth (MSE) retaining walls. Lightweight cellular concrete materials having four different unit weights were subjected to various amplitudes of sinusoidal waves at effective normal stresses ranging from 25 to 350 kPa. Results from this study show that the effective normal stress influenced the shear strength and stiffness more than the unit weight of the LCC materials. The backbone curves could be represented with a hyperbolic function, which can be developed for a known effective normal stress using the equations proposed in this paper. The maximum shear moduli of the LCC materials increased with a decrease in the unit weight and an increase in the effective normal stress. Likewise, the rate of reduction in normalized shear modulus (G/G_{max}) with strain also decreased with an increase in effective normal stress applied during seismic loading. Moreover, the damping ratio decreased with an increase in shear strain up to certain shear strain, which ranged from 0.25 to 0.35% for effective normal stresses of 25 and 350 kPa, respectively, and increased with shear strain after that transitional shear strain. The damping ratio of each type of LCC material tested was similar at the highest shear strain, i.e., 0.5% at a given effective normal stress. The results from this study can be used to evaluate the shear strength and deformation of the LCC materials in various geotechnical projects, such as in the backfill of MSE walls. **DOI: 10.1061/(ASCE)MT.1943-5533.0002155.**

Background

Construction on soft soils can pose a number of challenges for geotechnical engineers, including dealing with high amounts of consolidation settlement and low shear strengths, and bearing capacities. When these soft soils are located in seismic regions around the world, additional challenges arise, such as the amplification of seismic ground motions and, hence, an increased structural demand on the infrastructure (Pradel and Tiwari 2015). Traditionally, these poor ground conditions are improved with the implementation of costly ground modification techniques. However, the recent use of lightweight cellular concrete (LCC) in place of the existing weak soils is becoming more widespread. Particularly, LCC has been implemented as backfill for retaining walls and to absorb shocks around tunnels and pipelines in earthquake zones (LaVallee 1999). Mechanically stabilized earth (MSE) retaining walls with LCC backfills are found at several locations in California. A few examples are the Silicon Valley Berryessa Extension in San Jose, Colton Crossing for the Union Pacific–Burlington Northern Santa Fe (BNSF) railroad in Colton, and the San Bruno Railroad Grade Separation in San Bruno (Teig and Anderson 2012; Pradel and Tiwari 2015).

Lightweight cellular concrete is composed of a mixture of the traditional components of concrete (water, aggregates, and cement) and air voids. These air voids are established in the material via the introduction of either a protein-based or synthetic-based foaming agent that reacts mechanically and chemically with the other components to entrap the air (Maruyama and Camarini 2015; Panesar 2013; Tian 2011; Albayrak et al. 2007; LaVallee 1999). Because these materials can have between 10 and 70% air voids (Panesar 2013) depending on the amount of foaming agent introduced in the mixture, the materials can have unit weights as low as 3.1 kN/m^3 (The Aberdeen Group 1963).

Because LCC can provide several benefits, such as being lightweight, durable, noncorrosive, permanent, and stable, and have high freeze-thaw resistance, high insulating capacities, low water absorption, and low permeability, this material can be used in a number of geotechnical engineering applications (Maruyama and Camarini 2015; Tikalsky et al. 2004; LaVallee 1999; The Aberdeen Group 1963). Thus, it is important to understand how this material will behave under static and dynamic loading conditions. Several researchers have presented results related to a number of properties of this material under static conditions, including its thermal conductivity (Neville 2002; Narayanan and Ramamurthy 2000; Loudon 1979; The Aberdeen Group 1963), unconfined compressive strength (Zaidi et al. 2008; Narayanan and Ramamurthy 2000; LaVallee 1999), bearing capacity (LaVallee 1999), drying shrinkage (The Aberdeen Group 1963), thermal expansion (The Aberdeen Group 1963), water absorption capacities (Maruyama and Camarini 2015), and modulus of elasticity (Narayanan and Ramamurthy 2000). However, the dynamic properties of LCC has not been extensively studied and characterized.

In this paper, results obtained from the cyclic simple shear tests that were conducted on LCC specimens representing four different unit weight materials are presented. Specifically, the behavior of these materials pertinent to the maximum shear modulus, modulus reduction curves, and damping ratios is discussed in detail.

[1]Professor, Dept. of Civil and Environmental Engineering, California State Univ., Fullerton, 800 N. State College Blvd., E-419, Fullerton, CA 92834. E-mail: btiwari@fullerton.edu

[2]Assistant Professor, Dept. of Civil and Environmental Engineering, California State Univ., Fullerton, 800 N. State College Blvd., E-318, Fullerton, CA 92384 (corresponding author). E-mail: bajmera@fullerton.edu

[3]Engineer, Cell-Crete Corporation, 135 E. Railroad Ave., Monrovia, CA 91016. E-mail: dvillegas@cell-crete.com

Note. This manuscript was submitted on March 20, 2016; approved on August 2, 2017; published online on November 22, 2017. Discussion period open until April 22, 2018; separate discussions must be submitted for individual papers. This paper is part of the ***Journal of Materials in Civil Engineering***, © ASCE, ISSN 0899-1561.

Moreover, a discussion on the use of these properties in geotechnical engineering applications also is included.

Materials and Methods

Casting Procedures

The LCC materials used in this study were provided by the Cell-Crete Corporation (Monrovia, California). Two concurrent processes are used by the Cell-Crete Corporation to cast the LCC samples tested in this study. First, one part of a specific biodegradable protein-based surfactant (a by-product of the food industry) and 40 parts of water were mechanically agitated through a small nozzle to produce a foam, and subjected to compressed air action at a high air pressure. The use of different protein-based surfactants will produce LCC materials with varying unit weights. Second, on the basis of a specific mix design, cement and water were blended together to produce a neat cement slurry. This mixing process took place in a customized concrete mixer, which was coupled with a progressing cavity pump. Then, the neat cement slurry was used to produce an air-filled cellular concrete in a proprietary blending system with the addition of the preformed foam. The unit weight of the LCC was determined on the basis of the quantity of the preformed foam added to the neat cement slurry, and ranged from 3.14 to 18.9 kN/m^3. The LCC mixture then was poured into Styrofoam molds with the required dimensions to begin the curing process. In this study, five sets of samples were cast to a height of approximately 38.1 mm and a diameter of approximately 66.0 mm. Samples representing four different unit weights were cast. The details of the samples will be discussed subsequently.

Curing Process

After the LCC mixture was poured into the Styrofoam molds, the samples were allowed to set for 4 days. Between the 5th and 7th day after the pour date, the Styrofoam molds were cut carefully and the cast samples were removed. During this process, careful attention was paid to ensure that the samples were not accidently broken or cut. Each removed sample was wrapped in wet towels. These towels were soaked in deionized water for approximately 30 min prior to use. The wrapped LCC samples then were placed in an air-tight container, in which they were stored for 25 days after the pour date. The towels were moistened on a daily basis during this curing period. The wet towels and the lid to the air-tight container were removed on the 26th day after the pour date. For the next 3 days, that is, until the 28th day after the pour date, the LCC samples were allowed to air dry and continue curing. The trimming and testing of the samples took place on the 29th and 30th day after the pour date.

Fig. 1. Typical trimmed LCC sample prior to testing

Sample Trimming

For each cured sample, the height, weight, and diameter of the sample first were recorded. Using a Vernier Caliper (Aerospace, South El Monte, California), height measurements were taken at three different locations approximately 120° apart. A total of nine (three each at the top, middle, and bottom of the sample) diameter measurements were taken. Each sample also was weighed three times. These measurements were used to determine the moist unit weight of the specimen prior to trimming. After obtaining all of these measurements, the samples were carefully twisted into a ring with an inside diameter of 63.5 mm, such that the 25.4-mm tall ring was located at central 25.4 mm of the specimen. This twisting process trimmed the LCC sample to the required diameter. The portion of the specimen extruding outside the ring was carefully trimmed, on either side, using a frosted knife to obtain a specimen with a height of 25.4 mm. A typical trimmed LCC sample prior to testing is presented in Fig. 1. The height, weight, and diameter of the specimen was measured again following the procedure outlined previously. These measurements were used to compute the test unit weight of the specimen following the trimming procedures. The measured unit weights are outlined in the next section. The dry unit weight for each specimen was computed after the completion of cyclic simple shear testing using the weight measurements obtained after the specimen was placed in an oven for at least 24 h at a constant temperature of 110°C.

Unit Weight

Although the same the LCC batch mixture was used to cast each set of specimens, some differences in the unit weights of the specimens was expected. In this study, the unit weight of each specimen was determined prior to trimming, after trimming just prior to testing (or the test unit weight), and after 24 h of oven drying following the cyclic simple shear testing (or the dry unit weight). The range and average unit weights for each set of samples tested in this study are presented in Table 1. Table 1 shows that the average unit weight of the specimen prior to and after the trimming process was nearly the same; hence, it is safe to assume that the results

Table 1. Ranges of and Average Unit Weights for Tested Specimens

Batch description	Unit weight prior to trimming (kN/m^3)	Test unit weight (kN/m^3)	Dry unit weight (kN/m^3)
Class II–Batch 1	3.03–3.35 (average = 3.17)		Not measured
Class II–Batch 2	3.32–4.18 (average = 3.80)	3.52–4.12 (average = 3.91)	2.94–3.38 (average = 3.16)
Class IV	4.45–4.76 (average = 4.61)	4.62–4.79 (average = 4.71)	3.80–3.98 (average = 3.91)
7.1 kN/m^3 cast unit weight	5.55–6.68 (average = 6.24)	4.95–6.68 (average = 6.10)	4.20–5.74 (average = 5.06)
8.6 kN/m^3 cast unit weight	5.03–6.93 (average = 5.66)	5.03–7.37 (average = 5.64)	4.48–6.41 (average = 5.17)

J. Mater. Civ. Eng., 2018, 30(2): 04017271

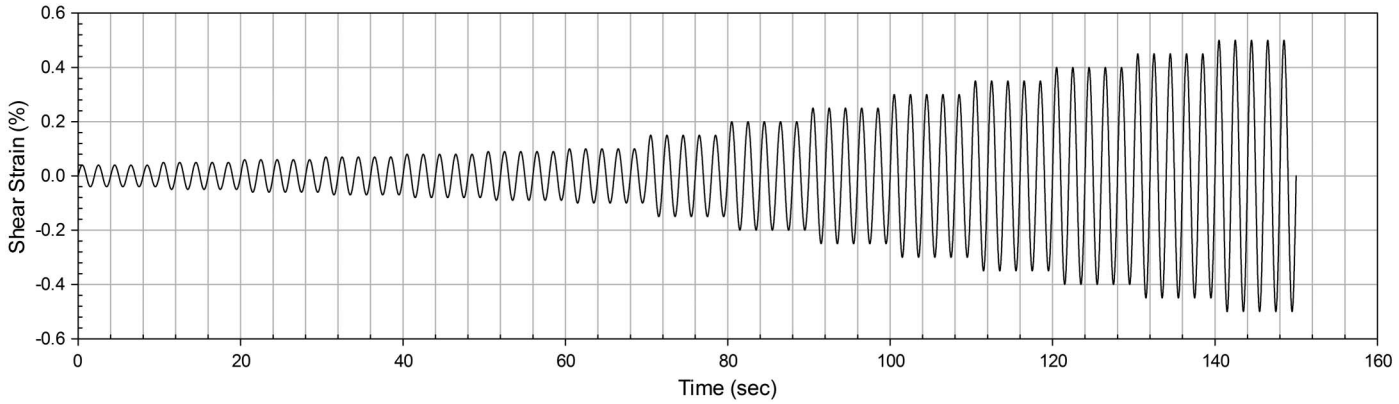

Fig. 2. Applied strain-controlled cyclic loading function

obtained in this study were not affected by the trimming procedures followed.

Cyclic Direct Simple Shear Testing

In this study, a Norwegian Geotechnical Institute (NGI)-type CDSS device, manufactured by GeoComp (Acton, Massachusetts), was used to conduct the cyclic direct simple shear (CDSS) testing (Dyvik et al. 1987; Bjerrum and Landva 1966). This automated, computer controlled apparatus uses a stack of 31 Teflon rings to confine the specimen laterally. Each Teflon ring is 0.94-mm thick. The horizontal loads were applied via a servo-motor; whereas, a microstepper motor was used to apply the vertical loads on the specimen. The CDSS device has both horizontal and vertical load capacities of 4,448 kN. In the horizontal direction, $\pm$12.5 mm displacement was permitted. Similarly, 12.5 mm of deformation was permitted in the vertical direction. Both the horizontal and vertical displacement readings were resolved to 0.0013 mm.

The trimmed LCC specimens were placed in a rubber membrane, confined by the stack of Teflon rings and secured in the cyclic simple shear apparatus. Then, the specimen was subjected to the desired consolidation pressure. At the end of the primary consolidation, determined from a real-time logarithm of time versus vertical deformation curve, the cyclic loading phase began. In this study, cyclic loading consisted of a series of different strain-controlled sinusoidal waves applied to the sample in undrained conditions. Each specimen was subjected to five cycles, each of 0.5-Hz frequency, of sinusoidal waves with strain amplitudes of 0.04, 0.05, 0.06, 0.07, 0.08, 0.09, 0.10, 0.15, 0.20, 0.25, 0.30, 0.35, 0.40, 0.45, and 0.50%. The test progressed through each of these amplitudes with no pauses between each step. The loading function applied is presented in Fig. 2. At the end of the cyclic loading phase, the specimen was removed from the cyclic simple shear device and placed into an oven for at least 24 h to determine its moisture content and dry unit weight. A total of 11 specimens were tested for each batch of LCC under four different consolidation pressures, i.e., 25 kPa (three specimens), 50 kPa (three specimens), 100 kPa (three specimens), and 350 kPa (two specimens).

A limitation of this study was the use of specimens that were 25.4 mm in height in all of the testing conducted. In the case of soft rock, surface fracture depends on the size of the specimen. These tests were conducted with the sample size specific to the testing equipment; larger size samples may yield slightly different results than those presented in the subsequent sections. A separate study is needed to evaluate the influence of the sample size on the dynamic behavior of the LCC materials.

Material Testing Results and Analysis

Although mechanical properties of the LCC materials also were measured with different static soil testing procedures, the details of those tests are not presented in this paper. Please refer to Tiwari et al. (2017), Tiwari and Ajmera (2015), and Maw and Cole (2015) for the testing methodology and study results pertinent to static soil tests. However, a summary of the mechanical properties of the LCC materials is presented in Table 2. For the purpose of comparison with other geomaterials, the friction angle of saturated loose sands typically ranges between 30° and 36°, whereas the friction angle for saturated dense sands is typically between 36° and 41°. Soft clays tend to have unconfined compressive strengths between 12.5 and 25 kPa, whereas stiff clays typically have unconfined compressive strengths between 50 and 100 kPa. The static properties of the materials will help to understand the dynamic behavior of the LCC materials. This paper primarily focuses on the dynamic properties of the LCC materials.

Stress-Strain Hysteresis Loops

A typical set of stress-strain hysteresis loops obtained from the CDSS test is presented in Fig. 3. The results in Fig. 3 are for a Class II–Batch 1 specimen under a consolidation pressure of 25 kPa. However, all of the specimens exhibited behavior similar to that shown in Fig. 2. The area of the hysteresis loop increased as the amplitude of the cyclic loading increased. The samples tested at higher consolidation pressures also exhibited similar behavior, but the area enclosed by the hysteresis loop at the same strain amplitude decreased. None of the hysteresis loops for any sample became open or banana-shaped.

Backbone Curves

The results obtained from the hysteresis loops were used to develop backbone curves for the LCC materials, as provided in Fig. 4, which represents a Class II–Batch 1 specimen tested at a consolidation stress of 25 kPa. In Fig. 4, the data points represent the peaks and troughs, corresponding to the points of stress reversal in the stress-strain hysteresis loops from Fig. 3. Also presented in Fig. 4, is a hyperbolic function as expressed in Eq. (1), which was fitted to these data points. In Eq. (1), τ is the shear stress, γ is the shear strain, whereas a and b are curve-fitting parameters. The CDSS apparatus is limited in measuring the cyclic shear stresses for shear strains less than 0.02%. However, as presented in Fig. 4, the hyperbolic function fitted well into the results provided by the CDSS for all samples. The maximum shear modulus (G_{max}) value was

Table 2. Mechanical Properties of the LCC Materials Used in This Study

Material	Unconfined compressive strength (kPa)	Friction angle for partially saturated conditions (degrees)	Cohesion for partially saturated conditions (kPa)	Friction angle for saturated conditions (degrees)	Cohesion for saturated conditions (kPa)	Undrained strength ratio	Hydraulic conductivity (cm/s)	At-rest earth pressure coefficient	Poisson's ratio
Class II–Batch 1	265–1,657	19	408	35	36	0.36–1.82	Not measured	Not measured	Not measured
Class II–Batch 2		20	187	35	36	0.28–1.54	1.7×10^{-4} to 7.7×10^{-4}	0.4–0.5	0.2–0.3
Class IV	628–2,765	21	615	35	36	0.48–1.80	1.2×10^{-3} to 9.5×10^{-4}	0.2–0.3	0.2–0.3
7.1 kN/m^3 cast unit weight	8,979–10,845	22	820	35	36	0.50–3.53	Not measured	Not measured	Not measured
8.6 kN/m^3 cast unit weight	10,729–13,406	21	1,174	35	36	0.54–1.89	Not measured	Not measured	Not measured

calculated by measuring the slope of the curve at axial strain of 0% by first calculating the derivative of the hyperbolic function and substituting γ as 0%. The shear wave velocities obtained from the CDSS for five samples was calculated on the basis of the value of G_{max}, obtained with the process outlined previously, one for each type of LCC material at 25-kPa consolidation pressure, matched well with the shear wave velocities obtained through bender element tests (Tiwari and Ajmera 2015). Fig. 5 contains several backbone curves for Class II–Batch 1 specimens tested with different consolidation stresses. This figure shows that the backbone curves shift upward as the consolidation pressure increased. Fig. 6 depicts the backbone curves for all types of LCC materials used in this study, in which upper and lower bounds referred to the Class II and 7.1-kN/m^3 cast unit weight LCC material, respectively, measured at the consolidation stress of 50 kPa. Close observation of all test data showed that the unit weight of the LCC had a very small influence on the backbone curves. Therefore, the results presented in Fig. 6 can be considered as the maximum and minimum ranges, and as average backbone curves for the LCC materials

$$\tau = \frac{a\gamma}{b + \gamma} \tag{1}$$

The values of parameters a and b in Eq. (1) can quantitatively provide additional insight into the behavior of the backbone curves. Eq. (1) shows that the parameter a scales the hyperbolic function such that an increase in a corresponds to an upward shift in the position of backbone curve. In this study, an increase in a would imply that a larger stress was required to cause the same amount of deformation in the LCC specimen. In contrast, slope of the hyperbolic function at a strain value of zero; thus, the curvature of the hyperbolic function is controlled by the parameter b. Specifically, an increase in the value of b implies that the curvature decreases. A higher value of b will imply that a lower shear stress is required to cause the same shear deformation.

Because Figs. 5 and 6 showed that there was a significant influence of the consolidation pressure and very small effect of the LCC unit weight on the backbone curves, the variation in the parameters a and b with the consolidation pressure was calculated and presented in Figs. 7 and 8, respectively. The bars in these figures represent the range of values for the parameters a and b across all specimens tested at any particular consolidation pressure. It shows that an increase in the consolidation pressure (σ_v') resulted in an increase in the value of a, which can be modeled by Eq. (2). Similarly, an increase in the consolidation pressure also resulted in an increase in the value of the parameter b. The best-fit regression line for the values of the parameter b with respect to the consolidation pressure is provided in Eq. (3). In Eqs. (2) and (3), the consolidation pressure should be expressed in kPa. Figs. 7 and 8 with Eqs. (2) and (3), respectively, suggest that as the consolidation pressure increased, the backbone curves for the LCC specimens shifted upward and tended to become less curved. Vertical solid lines presented in both Figs. 7 and 8, and in all subsequent figures, are the ranges of data and the solid circles are the average values

$$a = 0.4593\sigma_v' \tag{2}$$

$$b = 0.0027\sigma_v' + 0.0502 \tag{3}$$

Maximum Shear Modulus (G_{max})

The maximum shear modulus was calculated as the maximum slope of the backbone curve, which occurred at zero shear strain. The variation in the maximum shear modulus with the consolidation

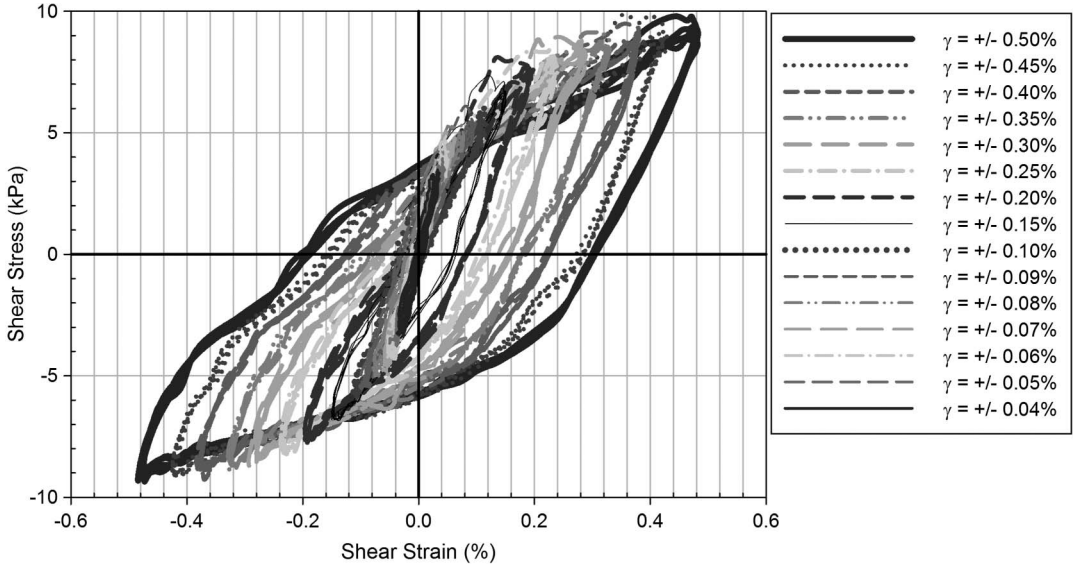

Fig. 3. Typical stress-strain hysteresis loops (a Class II–Batch 1 specimen with consolidation stress of 25 kPa)

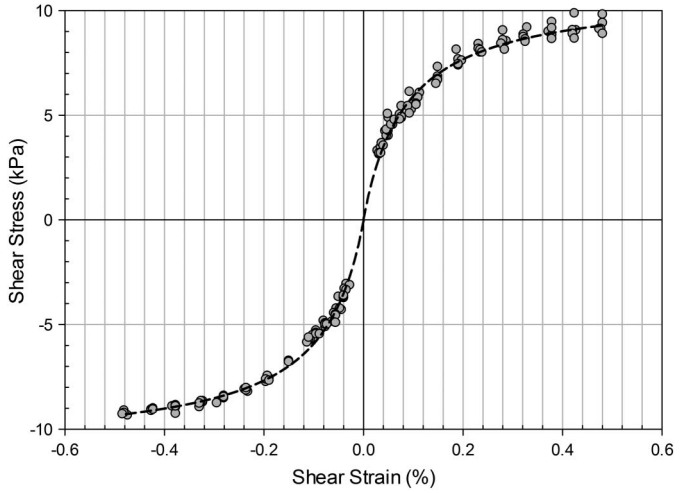

Fig. 4. Backbone curve for a Class II–Batch 1 specimen with consolidation stress of 25 kPa; data points represent the peaks and troughs of the stress-strain hysteresis loops presented in Fig. 3, whereas the line is the best fit hyperbolic function from Eq. (1) representing those data points

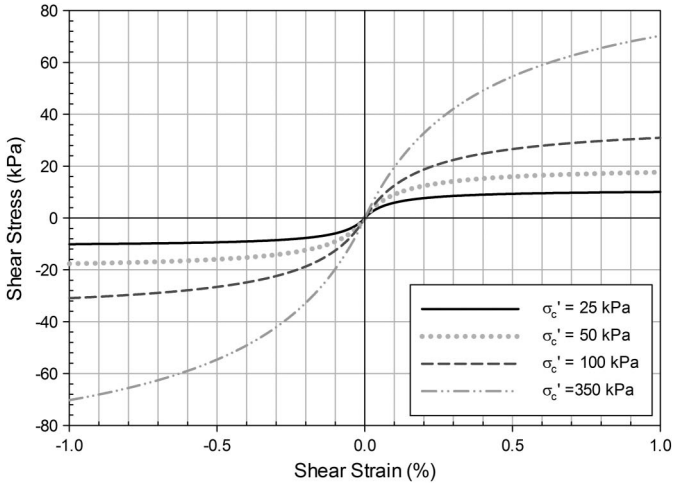

Fig. 5. Backbone curves for a Class II–Batch 1 specimens with different consolidation pressures

pressure is presented in Fig. 9. To compare the values of G_{max} for LCC materials with those for other geomaterials, AASTHO (1996) suggested that G_{max} range from 69 to 345 MPa for dense sands and gravels, from 27.6 to 138 MPa for silty sands, from 6.9 to 34.5 MPa for medium stiff clays, and from 27.5 to 137.5 MPa for soft clays. For all types of the LCC materials tested, the maximum shear modulus increased as the consolidation pressure increased. The increase in the maximum shear modulus with consolidation pressure was constant regardless of the unit weight of the material. The maximum shear modulus was highly dependent on the unit weight of the LCC materials and nearly independent of the consolidation stress, as presented in Fig. 10. The regression equations obtained from Figs. 9 and 10 are presented in Eqs. (4) and (5), respectively. The values of G_{max} and σ_v' are in kPa, and γ is in kN/m^3

$$G_{max} = 29.48\sigma_v' + 8{,}110.76 \quad (4)$$

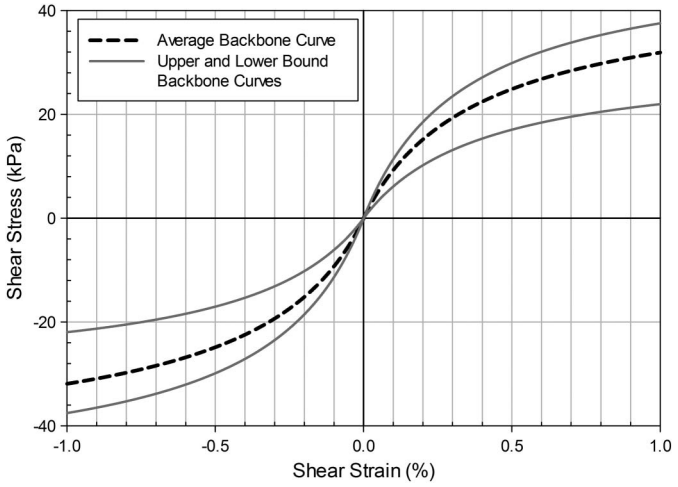

Fig. 6. Upper and lower ranges, and average backbone curves for all LCC specimens tested at a consolidation pressure of 50 kPa

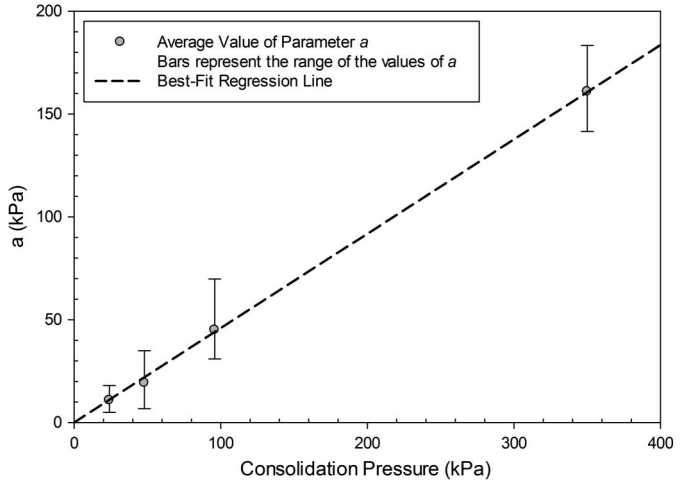

Fig. 7. Variation in parameter a of the hyperbolic function for backbone curves with consolidation pressure

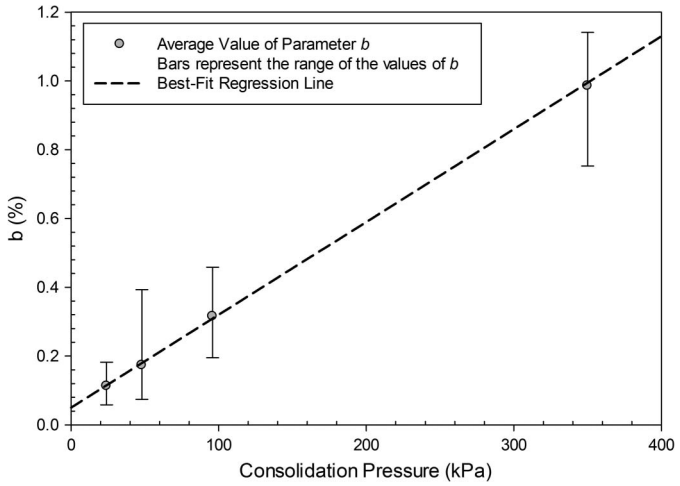

Fig. 8. Variation in parameter b of hyperbolic function for backbone curves with consolidation pressure

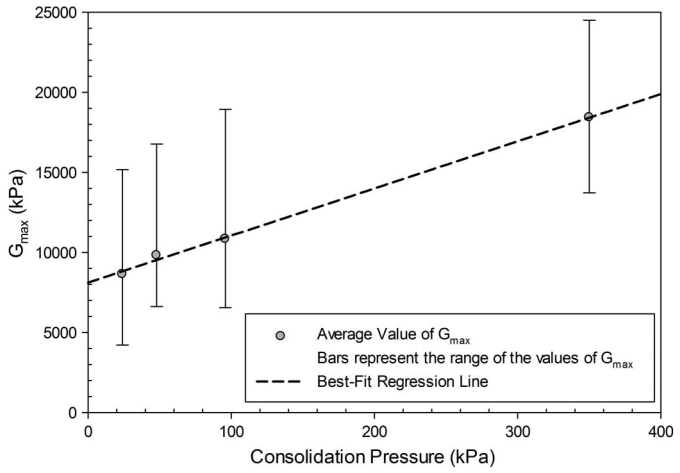

Fig. 9. Variation in the maximum shear modulus with the consolidation pressure

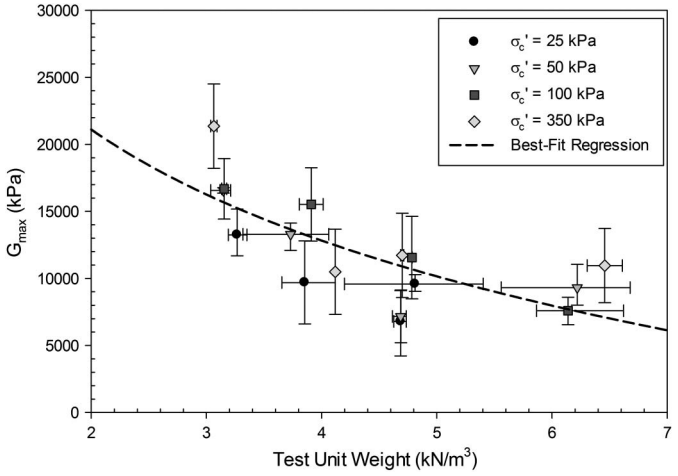

Fig. 10. Average reduction in maximum shear modulus for LCC materials having different unit weights tested at different consolidation pressures

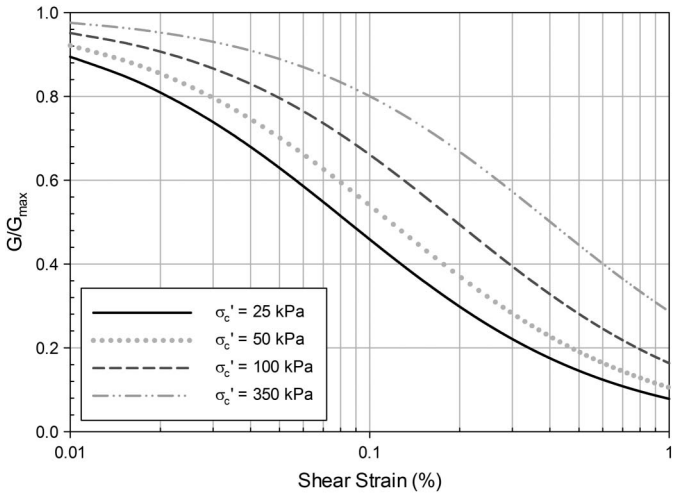

Fig. 11. Modulus degradation curves for Class II–Batch 1 samples at different consolidation pressures

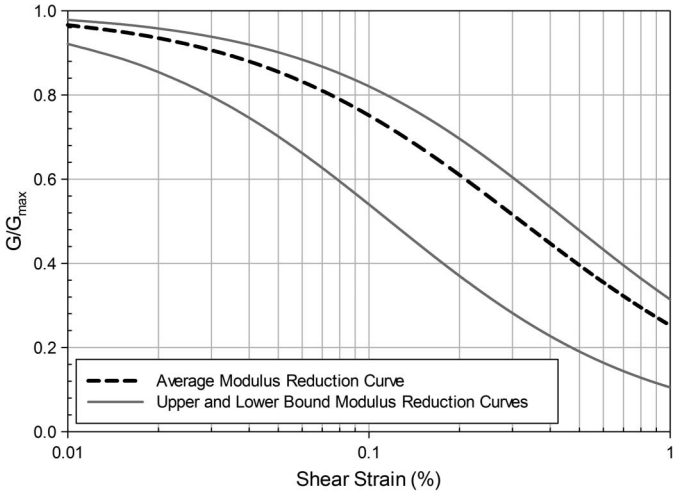

Fig. 12. Ranges and average modulus reduction curves for all lightweight cellular concrete specimens tested at a consolidation pressure of 100 kPa

$$G_{max} = 11{,}955\,\gamma + 29{,}400 \quad (5)$$

Modulus Reduction Curves

Fig. 11 contains a typical set of modulus reduction curves for LCC samples from Class II–Batch 1 at different consolidation pressures. At a constant shear strain, the ratio of the shear modulus to the maximum shear modulus (G/G_{max}) decreased as the consolidation pressure increased. Samples from different unit weights behaved in a manner similar to that shown in Fig. 11, although the results are not presented in this paper, but are available in Tiwari and Ajmera (2015). Similar to the behavior observed in the backbone curves,

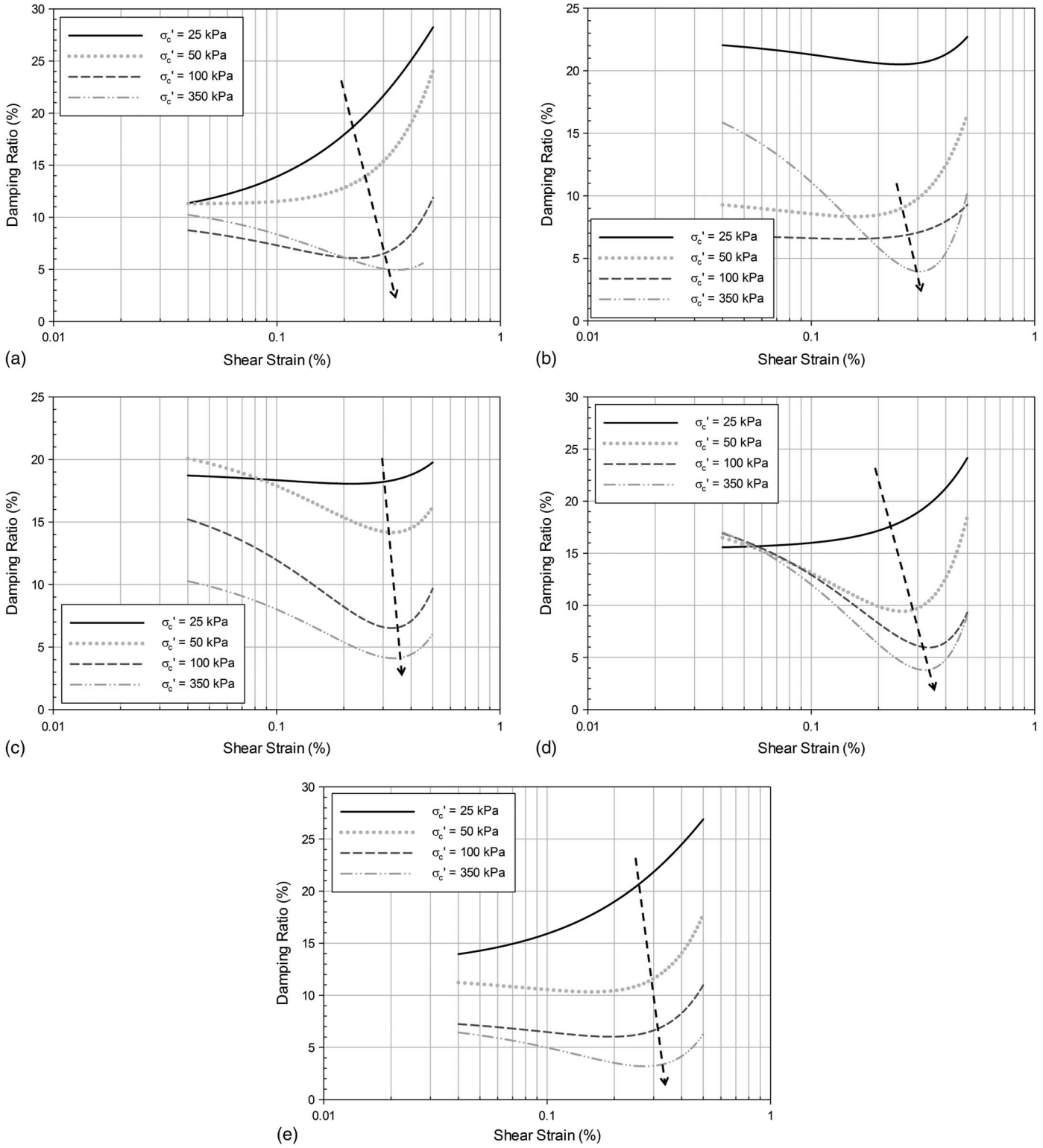

Fig. 13. Damping ratio versus shear strain for (a) Class II–Batch 1; (b) Class II–Batch 2; (c) Class IV; (d) 7.1 kN/m3 pour unit weight; (e) 8.6 kN/m3 pour unit weight LCC materials

close observation of the data showed that the unit weight of the LCC materials appeared to have little influence on the reduction in the shear modulus with respect to the shear strain experienced by the material. The ranges of modulus reduction curves for all the specimens tested at a consolidation pressure of 100 kPa and the curve for average values are presented in Fig. 12.

Damping Ratio

The results obtained from the CDSS test also were used to compute the damping ratios for the LCC specimens. Figs. 13(a–e) contains the variation in the damping ratio with shear strain separated on the basis of the consolidation pressure for each of the five sets of LCC specimens tested. Broken lines with arrows in Fig. 13 show the points of maximum curvature in each curve. The damping ratio was dependent on both the consolidation pressure and the shear strain. Fig. 13 shows that except for the samples consolidated at the effective stress of 25 kPa, there was a slight decrease in the damping ratio with an increase in the shear strain up to certain shear strains, generally between the shear strains of 0.25 and 0.35%, beyond which there was a significant increase in damping ratio with an increase in shear strain. The shear strain values corresponding to when the change in the mode of damping occurred was dependent on the consolidation pressure. Fig. 14 shows the variation of damping ratio with shear strain for all types of LCC materials tested at the consolidation stress of 50, 100, and 350 kPa. Samples behaved in a similar manner at other consolidation pressures as well. Broken lines with arrows in Fig. 14 show the points of maximum curvatures. These locations exhibited the strain in which the mode of damping ratio-shear strain relationship changed. Fig. 14 shows that except for one sample, the damping ratios of all samples at shear strain of 0.5% were similar, despite the unit weight of the LCC material. The cause for the difference in behavior in the Class II–Batch 2 sample was not obvious. Moreover, Fig. 14 shows that the majority of the samples exhibited a similar range of shear strains in which the damping ratio changed the mode, i.e., from a slight reduction in damping ratio to a significant increase in damping ratio with shear strain.

Discussion on the Dynamic Properties of LCC Materials

Figs. 5 and 7 illustrate that although the unit weight had a small influence, the effective vertical stress had a substantially larger effect on the dynamic shear strength of the LCC materials. On the contrary, the unit weight of the LCC materials played a significant role in the small strain stiffness of the LCC materials when compared with the effective vertical stress (Figs. 9 and 10). Moreover,

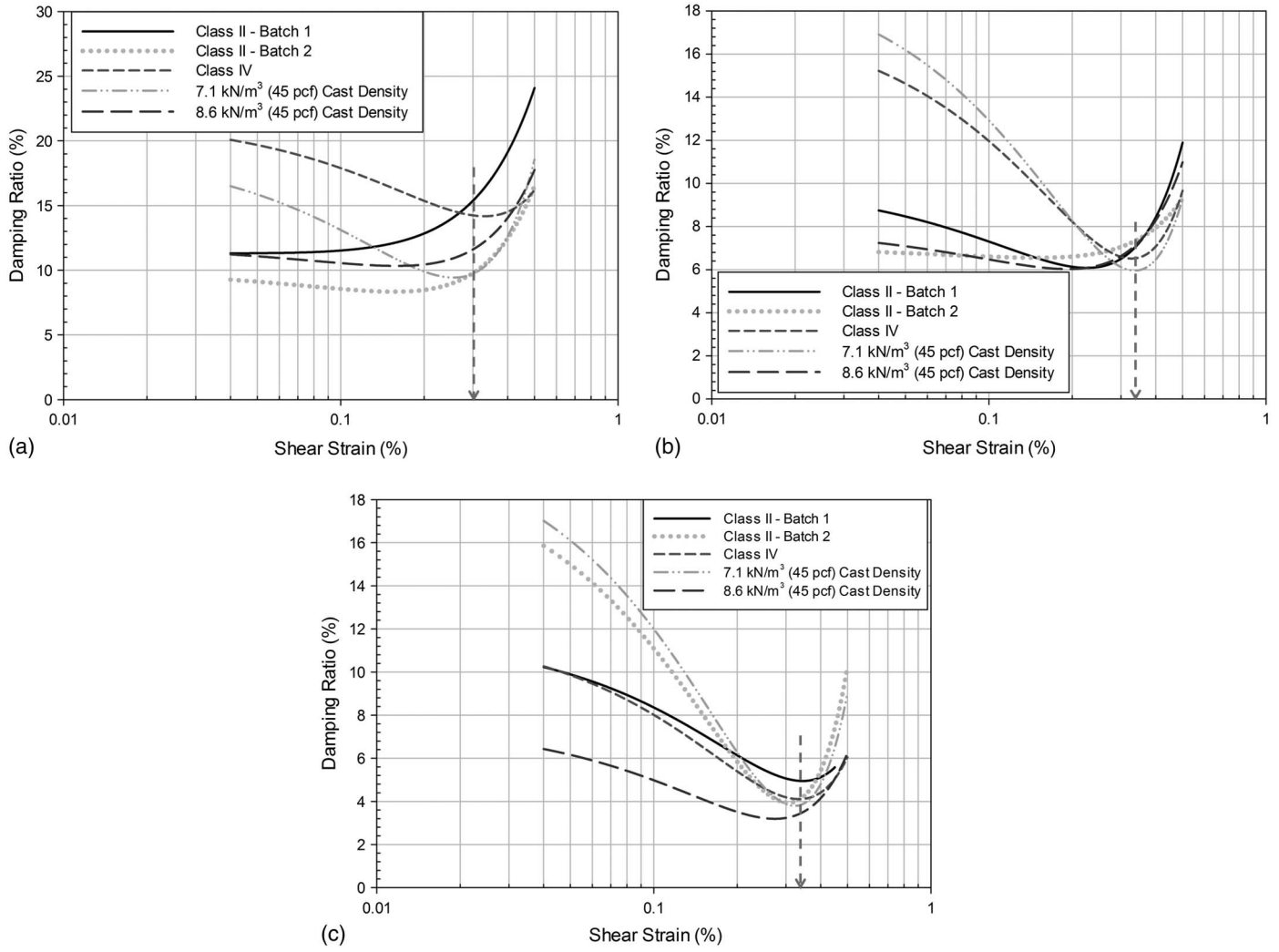

Fig. 14. Damping ratio versus shear strain for all types of LCC materials tested at consolidation pressure of (a) 50 kPa; (b) 100 kPa; (c) 350 kPa

significantly higher maximum shear moduli of LCC materials with lower unit weights in comparison with the higher unit weight materials implied that the low unit weight LCC materials were more advantageous in reducing the deformation during seismic events. Likewise, Figs. 11 and 12 show that the reduction in shear modulus with shear strain slightly decreased with an increase in effective vertical stress. This further supports the beneficial use of low unit weight LCC materials in various geotechnical applications, such as in the backfill of MSE walls.

As presented in Figs. 13 and 14, the damping ratio decreased with the shear strain up to certain values of shear strain, and then increased with shear strain. The shear strain at which such a transition occurred increases with the effective normal stress applied in the LCC materials, and ranged from 0.25 to 0.35% for the materials tested in this study. Trandafir and Erickson (2012) presented similar results for three different types of expanded polystyrene (EPS) materials. Although they discussed in the literature that the values of damping ratio decreased with an increase in axial strain, close observation of the data presented by Trandafir and Erickson (2012) shows that the damping ratio values increased with an increase in axial strain for axial strain values higher than 0.1–0.2%. The similarity in the unit weights of both of these materials can be attributed to the cause of the similarity in behavior between the EPS and LCC materials. The result obtained from this study for the LCC materials showed that for the shear strain that provided such transition for one specific effective normal stress, did not change significantly with the unit weight of the LCC material. Moreover, at the higher shear strains, the damping ratios remained similar for different unit weight LCC materials consolidated at the same effective vertical stress.

Summary and Conclusion

Lightweight cellular concrete materials have been used advantageously in civil engineering application for the past few decades. In this study, the dynamic properties of LCC materials with four different unit weights were measured using a fully automated CDSS device for the shear strains up to 0.5%. Specific attention was paid to evaluate the dynamic shear strength, stiffness, and damping of the materials at different effective vertical stresses, unit weights, and amplitudes of loading. The data analysis and results presented previously was helpful in arriving at the following conclusions:

1. The backbone curves representing the stress-strain relationship fit well with hyperbolic function presented in Eq. (1) for the strain range used in this study.
2. Shearing resistance with cyclic loading depended significantly on the effective normal stress applied. Larger shearing resistance was observed in the LCC materials consolidated and subjected to cyclic loading at higher normal stresses.
3. Although the dynamic shearing resistance increased slightly with unit weight, the effect of unit weight on the dynamic shearing resistance was very small compared with the influence of the effective normal stress on the dynamic shearing resistance.
4. The shape of the backbone curve depended significantly on effective normal stress. Using the relationships presented in Eqs. (2) and (3), the backbone curves can be developed for LCC materials at different effective normal stresses.
5. The maximum shear modulus increased with a decrease in unit weight of the LCC material and an increase in the effective normal stress. The values of maximum shear modulus can be estimated using Eqs. (4) and (5) for known unit weight and effective normal stress values.
6. Reduction in the shear modulus with the shear strain also was dependent on the effective normal stress.
7. Lightweight cellular concrete materials exhibited unique damping behavior with an increase in shear strain. Up to certain transitional shear strain, which in this study ranged from 0.25 to 0.35%, the damping ratio decreased with an increase in shear strain. Beyond this transitional shear strain, the damping ratio increased with shear strain. Such a transitional strain depended on the effective normal stress during dynamic loading and was found to increase with an increase in the effective normal stress.
8. The variation in the damping ratio with the shear strain was different for LCC materials with different unit weights at low values of shear strain. However, at shear strains of 0.5%, the damping ratios for all materials at any effective normal stress did not vary significantly with the unit weight of LCC materials.

Acknowledgments

Many individuals and organizations contributed to this project, and the authors would like to acknowledge their insight and assistance. In addition, several graduate students at California State University, Fullerton, including Miss Sneha Upadhyaya, Mr. Duc Tran, Mr. Janak Koirala, Mr. Prakash Khanal, and Miss Smriti Dhital, assisted in conducting the laboratory tests and in analyzing the data. Lab technician, Mr. Hector Zazueta, is thanked for his help in preparing and setting up the laboratory tests.

References

AASHTO. (1996). *Standard specification for highway bridges*, Washington, DC.

Albayrak, M., Yorukoglu, A., Karahan, S., Atlihan, S., Aruntas, H. Y., and Girgin, I. (2007). "Influence of zeolite additive on properties of autoclaved aerated concrete." *Build. Environ.*, 42(9), 3161–3165.

Bjerrum, L., and Landva, A. (1966). "Direct simple shear tests on a Norwegian quick clay." *Géotechnique*, 16(1), 1–20.

Dyvik, R., Berre, T., Lacasse, S., and Raadim, B. (1987). "Comparison of truly undrained and constant volume direct simple shear tests." *Géotechnique*, 37(1), 3–10.

LaVallee, S. (1999). "Cellular concrete to the rescue." *The Aberdeen Group Publication No. C99A039*, Hanley-Wood, Inc., Washington, DC.

Loudon, A. G. (1979). "The thermal properties of lightweight cellular concretes." *Int. J. Lightweight Concr.*, 1(2), 71–85.

Maruyama, R. C., and Camarini, G. (2015). "Properties of cellular concrete for filters." *Int. J. Eng. Technol.*, 7(3), 223–228.

Maw, R., and Cole, R. (2015). *Technical memorandum on laboratory testing of cellular concrete samples*, Gerhart Cole, Inc., Draper, UT.

Narayanan, N., and Ramamurthy, K. (2000). "Structure and properties of aerated concrete: A review." *Cem. Concr. Compos.*, 22(5), 321–329.

Neville, A. M. (2002). *Properties of concrete*, Pearson Education Limited, Harlow, U.K.

Panesar, D. K. (2013). "Cellular concrete properties and the effect of synthetic and protein foaming agents." *Constr. Build. Mater.*, 44, 575–584.

Pradel, D., and Tiwari, B. (2015). "The use of MSE walls backfilled with lightweight cellular concrete in soft ground seismic areas." *Proc., 3rd Int. Conf. on Deep Foundations*, Mexican Society for Geotechnical Engineering, Mexico.

Teig, J., and Anderson, J. (2012). "Innovative design for colton flyover grade separation of IPRR and BNSF, Colton, CA." *AREMA Annual Conf. and Exposition*, American Railway Engineering and Maintenance-of-Way Association, Lanham, MD.

The Aberdeen Group. (1963). *Cellular concrete*, Boston.

Tian, Y. (2011). "Experimental study on aerated concrete produced by iron tailings." *Adv. Mater. Res.*, 250, 853–856.

Tikalsky, P. J., Pospisil, J., and MacDonald, W. (2004). "A method for assessment of the freeze-thaw resistance of preformed foam cellular concrete." *Cem. Concr. Res.*, 34(5), 889–893.

Tiwari, B., and Ajmera, B. (2015). "Geotechnical properties of lightweight cellular concrete." *Research Rep. in Civil and Environmental Engineering Department*, California State Univ., Fullerton, CA.

Tiwari, B., Ajmera, B., Maw, R., Cole, R., Villegas, D., and Palmerson, P. (2017). "Mechanical properties of lightweight cellular concrete for geotechnical applications." *J. Mater. Civ. Eng.*, 10.1061/(ASCE)MT.1943-5533.0001885, 06017007.

Trandafir, A. C., and Erickson, B. A. (2012). "Stiffness degradation and yielding of EPS geofoam under cyclic loading." *J. Mater. Civ. Eng.*, 10.1061/(ASCE)MT.1943-5533.0000362, 119–124.

Zaidi, A. A. M., Rahman, A. I., and Zaidi, N. H. A. (2008). "Behavior of fiber reinforced foamed concrete: Indentation test analysis." *Proc., Seminar on Geotechnical Engineering*, Univ. Tun Hussein Onn Malaysia, Johore, Malaysia, 92–101.